



Shock compression response of high entropy alloys

Z. J. Jiang, J. Y. He, H. Y. Wang, H. S. Zhang, Z. P. Lu & L. H. Dai

To cite this article: Z. J. Jiang, J. Y. He, H. Y. Wang, H. S. Zhang, Z. P. Lu & L. H. Dai (2016) Shock compression response of high entropy alloys, *Materials Research Letters*, 4:4, 226-232, DOI: [10.1080/21663831.2016.1191554](https://doi.org/10.1080/21663831.2016.1191554)

To link to this article: <http://dx.doi.org/10.1080/21663831.2016.1191554>



© 2016 The Author(s). Published by Informa UK Limited, trading as Taylor & Francis Group.



Published online: 31 May 2016.



Submit your article to this journal [↗](#)



Article views: 805



View related articles [↗](#)



View Crossmark data [↗](#)



Citing articles: 2 View citing articles [↗](#)

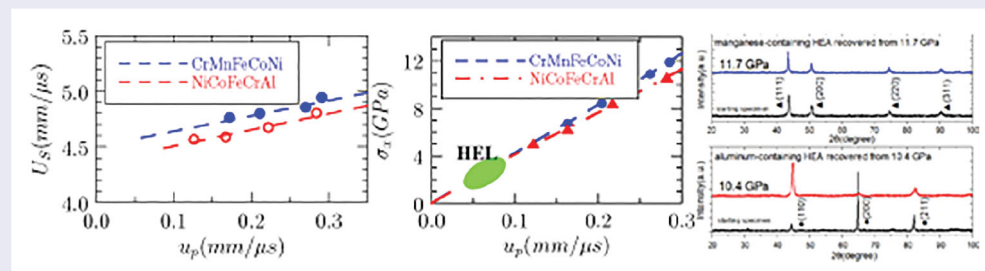
Shock compression response of high entropy alloys

Z. J. Jiang^a, J. Y. He^b, H. Y. Wang^a, H. S. Zhang^a, Z. P. Lu^b and L. H. Dai^a

^aState Key Laboratory of Nonlinear Mechanics, Institute of Mechanics, Chinese Academy of Sciences, Beijing, People's Republic of China; ^bState Key Laboratory for Advance Metals and Materials, University of Science and Technology Beijing, Beijing, People's Republic of China

ABSTRACT

In this work, we studied the shock response of two typical equiatomic high entropy alloys (HEAs) (i.e. FCC-structured CrMnFeCoNi alloy and BCC-structured NiCoFeCrAl alloy). The experimental results show that these two HEAs exhibit a relatively high Hugoniot elastic limit and high-phase transition threshold stress. We attribute this anomalous dynamic response of HEAs to their intrinsic chemically disordered structures. This work may provide new insight into shock compression behavior of HEAs.



IMPACT STATEMENT

This is the first work to demonstrate that high entropy alloys (HEAs) behave 'super-stably' under shock loading, which may provide new insight into shock compression behavior of HEAs.

ARTICLE HISTORY

Received 9 March 2016
Revised 1 May 2016
Accepted 16 May 2016

KEYWORDS

High entropy alloy; dynamic compression; equation of state

1. Introduction

Recently, a new type of metallic alloys containing four or more elements in equiatomic ratios, referred to as HEAs, emerged and has attracted increasing attention due to their unique composition, structure and properties.[1–15] This novel alloy design strategy of configurational entropy maximization can render HEAs to form a simple phase structure, and possess high thermal stability and good mechanical properties.

One of the greatest merits of HEAs is their good potential to achieve favorable mechanical properties. Ritchie, George and their coworkers [10,11,16] showed that the FCC-structured CrMnFeCoNi HEA has a unique combination of mechanical properties compared with conventional alloys, such as cryogenic steels. The fracture toughness of this HEA maintains a high level even at cryogenic temperatures, associated with an enhancement in tensile strength and ductility. HEAs have great potential to be the most damage-tolerant materials in a wide temperature range and an ideal material for cryogenic applications.

Wang et al. [17–19] demonstrated that the yield strength of the BCC-structured NiCoFeCrAl HEA is rather high under quasi-static compression, which is comparable to bulk metallic glasses (BMGs). Mishra et al. [20,21] studied the deformation behavior of Al_{0.1}CrFeCoNi HEA, and their results demonstrated the high strain-rate sensitivity of yield stress of HEA. Moreover, the dynamic deformation mechanism of HEA is completely different from conventional crystalline alloys with similar composition, such as austenitic stainless steels and high-Ni steels.[22]

The excellent mechanical and physical properties of HEAs,[1,3,23,24] such as high damage tolerance in a wide temperature range, promising fatigue resistance and good wear resistance, render them potential candidates as structural materials in aerospace, defense and high-speed manufacture industry. Therefore, the shock properties of HEAs at ultra-high strain rate are highly needed. As in previous studies, topologically disordered BMGs exhibit an anomalous dynamic response under shock

compression, which suggests that the dynamic response of materials is strongly influenced by the microscopic configuration.[25–28] As the multiple-element mixture in HEA systems tends to cause severe lattice distortion, both the chemically disordered HEAs and topologically disordered BMGs possess a disordered nature in microscopic configuration. Therefore, a fundamental question arises: How does the severe microscopic lattice distortion affect the dynamic properties of chemically disordered HEAs? However, at present, there is no work reported on the dynamic response of HEAs under shock compression. As HEAs have great potential to be an ideal material for various applications in dynamic engineering fields, studies on the dynamic response of HEAs under shock compression is of considerable interest not only scientifically but also technologically.

2. Experimental Procedure

In our work, two typical equiatomic HEAs, that is, FCC-structured CrMnFeCoNi and BCC-structured NiCoFe-CrAl alloy, were chosen to be the target materials, as these alloys possess simple but totally different phase structures, and their static properties have been studied extensively.[10,11,16,17,29,30] Ingots of the HEAs were obtained by arc-melting a mixture of pure metals (purity > 99 wt.%) in a Ti-gettered high-purity argon atmosphere, and remelted seven times to ensure chemical homogeneity. The ingots were subsequently drop-cast into a copper mold, and the details regarding the casting process can be found in literature.[31] The nominal density used in present study was measured by the Archimedean method. The longitudinal wave speed was determined via ultrasonic pulse-echo technique at the National Institute of Metrology of China, and the Poisson's ratio was obtained from previous studies.[10,29] For FCC-structured manganese-containing HEA, the Poisson's ratio, average density and longitudinal wave speed were determined to be 0.266, 7.856 g/cm³ and 5,780 m/s, respectively, while for the BCC-structured aluminum-containing HEA, those values were 0.309, 7.030 g/cm³ and 6,080 m/s. The grain sizes of FCC-structured HEA and BCC-structured HEA were about 400 μm and 330 μm, respectively.

A series of normal plate impact experiments was performed with a Φ101 mm diameter one-stage light gas gun at the Institute of Mechanics, Chinese Academy of Sciences. The experimental configuration [32–34] is schematically illustrated in Figure 1. The projectile, viz., a flyer plate made of standard material backed with a low-impedance polycarbonate base plate, was driven by the high-pressure nitrogen to impact the HEA target plate. In

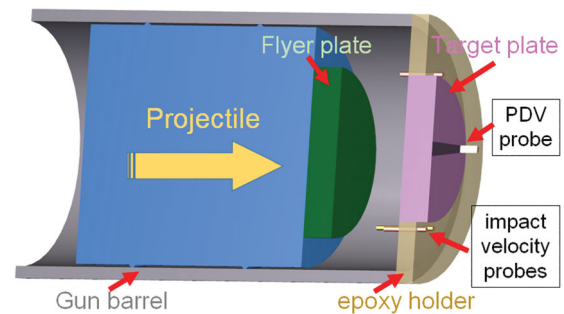


Figure 1. Schematic of the normal plate impact experiments.

our experiments, a set of standard materials (i.e. oxygen-free high-conductivity copper and 6,061 aluminum alloy) with contrasting wave impedance was selected in order to achieve different impact states. The dynamic properties of these standard materials were reported in Refs. [35,36]. To facilitate the analysis of wave interaction, the flyer plates were thick enough so that the interaction of the release wave in the flyer plate could be ignored. Both the specimens and the flyer plates were finished in parallel to an accuracy of 5 μm to ensure the generation of the plane wave after impact. As illustrated in Figure 1, a photonic Doppler velocimetry system [37] was adopted to measure the velocity of the free surface, and a pair of coaxial electric probes was embedded in the epoxy holder to record the impact velocity. In the experiments, the ‘soft recovery’ technique was adopted. A steel cylinder was placed at the back of the vacuum chamber, which could stop the large flyer plate, but allow the passage of the small target plate. The target sample was soft recovered by decelerating into several stages of cotton drags.

To study the microstructure changes of the post-shocked samples, the microstructure of the original and soft-recovered specimens was characterized using X-ray diffraction (XRD) with $K\alpha$ -Cu radiation and transmission electron microscopy (TEM). For TEM observations, thin samples with an initial thickness of 0.5 mm were cut from the soft-recovered specimens using a wire electrical discharge machining, and reduced to less than 0.04 mm thick by mechanical grinding, then punched into standard 3 mm diameter TEM discs, and thinned by ion milling.

3. Results and Discussions

Figure 2 shows the measured free surface velocity profiles of eight shots. The material is initially loaded by an elastic precursor wave which propagates with the longitudinal sound speed, and the Hugoniot elastic limit (HEL) is the stress amplitude of the elastic precursor, which represents the maximum normal stress that a material can withstand

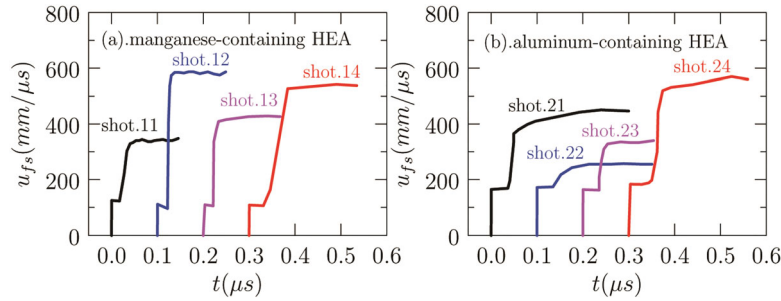


Figure 2. The measured free surface particle velocity profiles of HEA samples. (a) manganese-containing HEA and (b) aluminum-containing HEA.

Table 1. Summary of experiments on FCC-structured manganese-containing HEA target.

shot.No	Impactor			Target sample					
	Material	Thickness mm	Impact Velocity mm/ μ s	Thickness mm	HEL GPa	u_p mm/ μ s	σ_{peak} GPa	U_S mm/ μ s	$\bar{\epsilon}$ 1/ μ s
11	Aluminum	2.76	.588	1.031	2.85	.172	6.88	4.77	4.63
12	OFHC	2.76	.588	1.022	2.53	.291	11.68	4.94	4.83
13	OFHC	10.84	.425	0.981	2.50	.212	8.40	4.79	4.88
14	OFHC	2.29	.544	0.925	2.38	.270	10.70	4.85	5.24

under one-dimensional compressive strain without plastic deformation at ultra-high strain rate.[38] As the elastic precursor may decay along with its propagation, the measurement of the HEL was conducted only on a 1 mm thick target so that the attenuation in HEL could be ignored. The measured HELs are listed in Table 1 and Table 2.

Comparing with the conventional crystalline alloys of a similar composition, HEAs show a relatively high Hugoniot elastic limit besides exhibiting unexpectedly high damage tolerance and promising fatigue resistance. [10,11] The average HELs of the FCC-structured manganese-containing HEA and BCC-structured aluminum-containing HEA are determined to be 2.58 GPa and 3.70 GPa, respectively, significantly higher than those of traditional crystalline alloys with similar composition,[36] such as the FCC-structured austenitic stainless steel (1.4 GPa) and HY80 naval armor steel (1.7 GPa).

Beyond the HEL, the free surface velocity steeply rises to the peak velocity, corresponding to the arrival of plastic wave. In this work, the free surface approximation and impedance-matching method [28,32,34] have been adopted in determining the shock Hugoniot of the peak

state. In addition, the nominal strain rates averaged over thickness are estimated by $\bar{\epsilon} = U_S/L$. The plastic wave velocities and the nominal strain rates of HEA samples are listed in Table 1 and Table 2.

The shock Hugoniot data (shock velocity U_S versus particle velocity u_p) for the HEAs are plotted in Figure 3. After careful examination of the experimental data, we found that in plastic region, the shock velocity U_S follows the general linear relationship with the particle velocity u_p , as shown in Figure 3. That is,

$$U_S = c_0 + s u_p,$$

where c_0 and s are the sound velocity in the material at zero pressure and the linear Hugoniot slope coefficient, respectively. The values of c_0 and s for the two HEAs are listed in Table 3.

According to the Dugdale and Macdonald's approximation,[39] the Gruneisen parameter γ can be deduced from $\gamma = 2s - 1$. Gruneisen coefficient γ is a key parameter in the Gruneisen equation of state, which represents the change of pressure with internal energy in unit volume under isometric condition.[40]

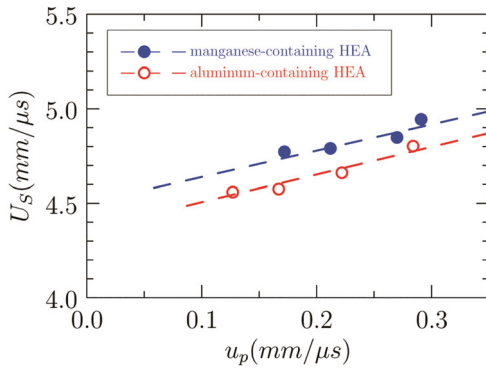
Table 2. Summary of experiments on BCC-structured aluminum-containing HEA target.

Material shot.No	Impactor		Target sample						
	Thickness mm	Impact Velocity mm/ μ s	Thickness mm	HEL GPa	u_p mm/ μ s	σ_{peak} GPa	U_S mm/ μ s	$\bar{\epsilon}$ 1/ μ s	
21	OFHC	2.76	.434	1.081	3.51	.222	8.14	4.66	4.31
22	Aluminum	2.76	.434	1.064	3.71	.127	4.98	4.56	4.28
23	Aluminum	2.76	.550	1.068	3.50	.167	6.29	4.58	4.29
24	OFHC	2.76	.550	1.075	3.90	.284	10.37	4.80	4.47

Table 3. The dynamic properties of HEAs.

	Components	HEL (GPa)	c_0 (mm/ μ s)	s	γ^a
Manganese-containing HEA	CrMnFeCoNi	2.58	4.50	1.39	1.78
Aluminum-containing HEA	NiCoFeCrAl	3.70	4.36	1.46	1.92

^aThe Gruneisen parameter was determined from Dugdale and Macdonald's approximation.

**Figure 3.** U_S – u_p Hugoniot results of the manganese-containing HEA and aluminum-containing HEA.

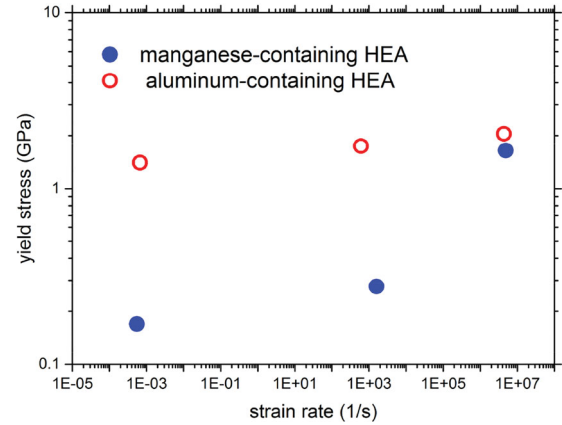
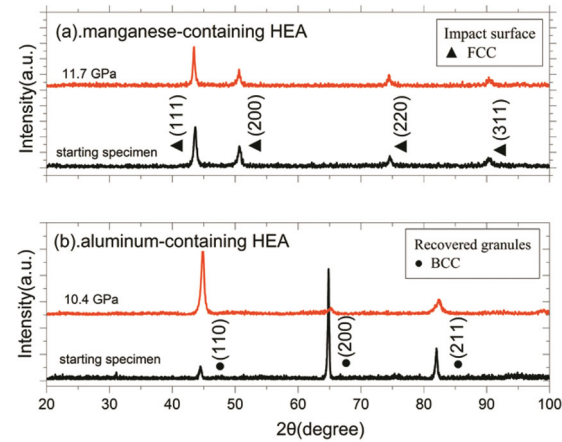
In our experiments, the values of γ are listed in Table 3.

According to the von Mises yield criterion,[40] the elastic limit under uniaxial strain condition σ_H is directly related to the shock yield stress σ_Y under uniaxial stress state as

$$\sigma_Y = \sigma_H \frac{1 - 2\nu}{1 - \nu},$$

where ν is the Poisson's ratio. The corresponding shock yield stress in uniaxial stress state of the manganese-containing HEA and aluminum-containing HEA are 1.64 GPa and 2.05 GPa while the strain rate is around $5.0 \times 10^6/s$. However, in quasi-static compression tests (strain rate around $5.0 \times 10^{-4}/s$), the yield stress are only about 0.17 GPa for manganese-containing HEA and 1.40 GPa for aluminum-containing HEA, and in SHPB experiments (strain rate around $1.0 \times 10^3/s$), the dynamic yield stress of these two HEAs are 0.27 GPa and 1.74 GPa, respectively. The yield stress of these two typical HEA samples exhibit rate dependence, especially the manganese-containing HEA, as shown in Figure 4. Obviously, the shock yield stress of manganese-containing HEA increase significantly under ultra-high strain rate, which suggests the substantial change in its deformation mechanism.

Under plate impact, if there is a phase transformation in the target material, the plastic wave and phase transition wave may separate in the target plate, which induces multiple plateaus in free surface velocity profile. It is noticeable that for all these eight shots in this study, the two-wave structure in the free surface velocity profile suggests that no phase transition occurs at stress below

**Figure 4.** The effects of strain rate on the yield stress of two typical HEAs.**Figure 5.** XRD patterns of the original and recovered samples (a) manganese-containing HEA samples (b) aluminum-containing HEA samples.

11 GPa in both HEAs. As we know, conventional crystalline alloys of similar composition (Fe, Mn, Ni, etc.) possess a relative low martensitic transformation threshold, which is about 6 GPa. Since the target plates are very thin, it might be quite difficult to resolve the phase transition signals in the free surface velocity profile. Further microstructural characterizations were carried out on the soft-recovered samples to search for the evidence of phase transition.

Figure 5 compares the XRD patterns of the original and the soft-recovered samples after the 11.7 GPa shot for manganese-containing HEA and 10.4 GPa shot for aluminum-containing HEA. For FCC-structured

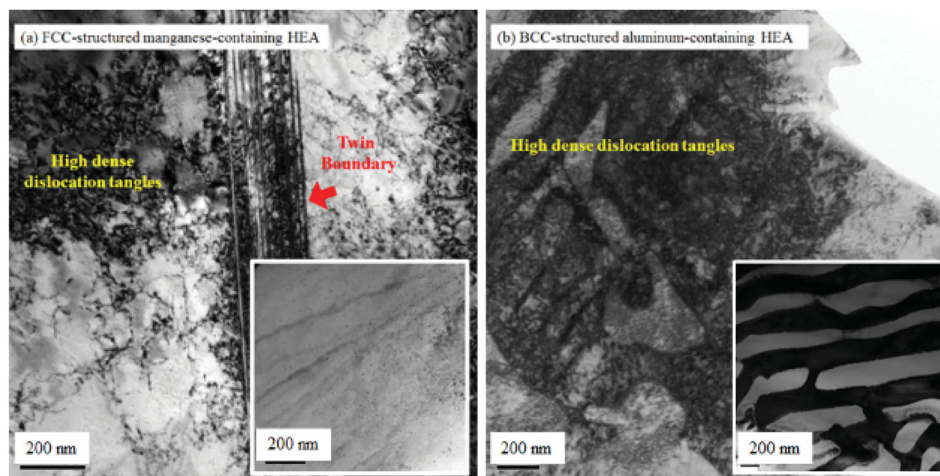


Figure 6. TEM images showing different microstructural features in the deformed and undeformed samples: (a) comparison between the pre-loading manganese-containing HEA sample and sample recovered from 11.7 GPa; (b) comparison between the pre-loading aluminum-containing HEA sample and sample recovered from 10.4 GPa.

manganese-containing HEA, the X-ray diffraction were conducted on the impact surface of the recovered specimen discs. As the BCC-structured aluminum-containing HEA specimens broke into many fragments under shock compression, the X-ray diffraction were conducted on the recovered granules. In both the XRD patterns, the characteristic diffraction peaks change little. Hence, for both FCC-structured manganese-containing HEA and BCC-structured aluminum-containing HEA, the recovered specimens maintain their original phase structures, which confirms that no martensitic transformation occurred below 11 GPa.

TEM images also confirm that no martensitic transformation occurred in the specimens under shocks below 11 GPa. Figure 6 shows the bright-field TEM images of the deformed and undeformed samples, and the deformed samples were soft recovered from the 11.7 GPa shot and 10.4 GPa shot. In the TEM images of undeformed manganese-containing HEA, only few dislocations and stack faults were observed, while the deformed manganese-containing FCC HEA samples show high-density tangled dislocations, extensive deformation twinning and heavily banded microstructures, termed as deformation bands, as depicted in Figure 6(a). These deformation bands might be regions containing either very narrow twins or stacking faults, which are common in low Stacking Fault Energy alloys. It should be noted that for manganese-containing HEA samples, intensive twinning was only observed in the recovered samples after high strain-rate test; the quasi-statically deformed samples at room temperature did not exhibit any twinning.[20] The profusion of dislocations and twins confirm that in the FCC-structured manganese-containing HEA, dislocation motion and twinning are

the dominant mode of plastic deformation at ultra-high strain rate. In the undeformed aluminum-containing HEA, only very low densities dislocations were observed. However, in the aluminum-containing HEA samples soft recovered from ultra-high strain rate shots, only high-density tangled dislocations, no visible twinning, were observed, as shown in Figure 6(b). Hence, dislocation motion is the dominant mode of plastic deformation in the BCC-structured aluminum-containing HEA under impact loading. For either the post shocked manganese-containing HEA or aluminum-containing HEA samples, no martensite formation was observed, which means these HEAs possess an enhanced phase transition threshold.

The measured free surface velocities profiles, the XRD patterns and the TEM images of the recovered samples prove that no phase transition occurred in the shots under 11 GPa. Hence, for both the manganese-containing HEA and aluminum-containing HEAs, the phase transition threshold stress is significantly higher than 11 GPa.

Compared with the conventional crystalline alloys of similar composition, these HEAs possess an enhanced phase transition threshold. Although the phase transition stress of pure iron is around 13 GPa, the threshold stress decreases with the addition of manganese and nickel, as exhibited in Ref. [41]. For instance, the transition stress of simple binary Fe–Mn alloys dramatically drops to 6 GPa while the mass fraction of manganese exceeds 10%, and for FeMnNi alloy, the martensitic transformation threshold is only 6.3 GPa.[38] However, to our surprise, for HEA systems, even with more addition of both Mn and Ni to 20%, respectively, their transition stress is still significantly high, manifesting that HEAs

are more stable than the conventional alloys with similar composition.

The TEM images provide hints for the much higher shock yield stress in the aluminum-containing HEA. As shown in the TEM bright-field image of pre-loading microstructures in Figure 6, the aluminum-containing HEA spinodally decomposes into modulated plate structure of the Al-rich BCC phase and the Cr-rich BCC phase,[17] while the manganese-containing HEA consists of only one simple phase. As the width of the shock front is in the same order as the spinodal decomposition structures, the spinodal decomposition structure can be considered as effective barriers of slip dislocations as grain boundaries, which could cause significant precipitation strengthening in the yield stress, and the nano-spaced spinodal structure would also produce a nano-composite strengthening effect.[1] These multi-strengthening mechanisms are expected to be responsible for the much higher shock yield stress of the aluminum-containing HEA.

At ultra-high strain rate, the dislocation velocity v is controlled by the applied shear stress τ and the friction forces f_v according to $f_v = Bv = b\tau$, where B is the drag coefficient and b is the Burgers vector. With the increasing of the imposed strain rate, the moving velocity of mobile dislocations could approach shear wave velocity. In such situation, the relativistic effects will dramatically increase the matter viscosity by $B = B_0/(1 - v^2/C_S^2)$, where B_0 the drag coefficient at rest.[40] Therefore, it requires a higher stress for the onset of the dislocation motion at ultra-high strain rate, which leads to the significant rise in yield strength. However, aluminum is strain rate insensitive at ultra-high strain rate.[42] Hence, the rate sensitivity of HEA containing 20% aluminum is lower than that of manganese-containing HEA, as demonstrated by our data.

In our view, the anomalous high HEL under impact can be attributed to the microscopic configuration of HEAs. As HEAs possess severe local lattice distortion, which leads to the formation of a large local elastic stress field, the interactions between these local elastic stress fields and the stress field of dislocations will hinder dislocation movements in HEAs. Thus, compared with traditional crystalline alloys with similar composition, HEAs exhibit higher frictional stress in the motion of dislocations. Under shock loading, the moving velocity of mobile dislocations could approach shear wave velocity; under such conditions, the relativistic effects would cause increment in the matter viscosity, and thus it requires a higher onset stress for movement of dislocations. Hence, HEAs could possess an anomalously high dynamic yield stress under shock compression. In addition, the severe lattice distortion and high confine pressure could inhibit

the local atomic rearrangement process,[43] which could greatly enhance the activation energy for phase transition and hence, increase the resistance to phase transition. Therefore, HEAs possess relatively both high HEL and high-phase transition threshold stress under plate impact.

4. Conclusion

In this study, the planar impact experiments were performed on two typical HEAs and the dynamic responses of the HEAs were determined. Both HEAs showed exceptionally high HELs and phase transition stress. We attribute this anomalous dynamic response to their intrinsic chemically disordered structures. Our findings may provide new insight into shock compression behavior of HEAs.

Acknowledgements

The authors thank F. F. Shi, X. L. Wang, L. T. Shen, Y. L. Deng for the experimental assistance.

Disclosure Statement

No potential conflict of interest was reported by the authors.

Funding

This work was supported by the National Basic Research Program of China [Grant No. 2012CB937500], and the National Natural Science Foundation of China [Grant Nos. 11172311, 11021262, 10932011, 11472287, 51531001].

References

- [1] Yeh JW, Chen SK, Lin SJ, et al. Nanostructured High-Entropy Alloys with Multiple Principal Elements: Novel Alloy Design Concepts and Outcomes. *Adv Eng Mater.* 2004;6(5):299–303.
- [2] Cantor B, Chang ITH, Knight P, Vincent AJB. Microstructural development in equiatomic multicomponent alloys. *Mater Sci Eng: A.* 2004;375–377:213–218.
- [3] Zhang Y, Zuo TT, Tang Z, et al. Microstructures and properties of high-entropy alloys. *Prog Mater Sci.* 2014;61:1–93.
- [4] Santodonato LJ, Zhang Y, Feyngenson M, et al. Deviation from high-entropy configurations in the atomic distributions of a multi-principal-element alloy. *Nat Commun.* 2015;6:5964–13.
- [5] Yeh JW. Alloy design strategies and future trends in high-entropy alloys. *JOM.* 2013;65(12):1759–1771.
- [6] Miracle DB, Miller JD, Senkov ON, Woodward C, Uchic MD, Tiley J. Exploration and development of high entropy alloys for structural applications. *Entropy.* 2014;16(1):494–525.
- [7] Guo S, Ng C, Lu J, Liu CT. Effect of valence electron concentration on stability of fcc or bcc phase in high entropy alloys. *J Appl Phys.* 2011;109(10):103505–5.

- [8] Wu Y, Liu WH, Wang XL, et al. In-situ neutron diffraction study of deformation behavior of a multi-component high-entropy alloy. *Appl Phys Lett*. 2014;104(5):051910–5.
- [9] Tsai MH, Zhu YT, Yeh JW, et al. Morphology, structure and composition of precipitates in $\text{Al}_{0.3}\text{CoCrCu}_{0.5}\text{FeNi}$ high-entropy alloy. *Intermetallics*. 2013;32:329–336.
- [10] Gludovatz B, Hohenwarter A, Catoor D, Chang EH, George EP, Ritchie RO. A fracture-resistant high-entropy alloy for cryogenic applications. *Science*. 2014;345(6201):1153–1158.
- [11] Zhang Z, Mao MM, Wang J, et al. Nanoscale origins of the damage tolerance of the high-entropy alloy CrMnFeCoNi. *Nat Commun*. 2015;6:10143–6.
- [12] Tsai MH, Yeh JW. High-entropy alloys: a critical review. *Mater Res Lett*. 2014;2(3):107–123.
- [13] Zhao YJ, Qiao JW, Ma SG, et al. A hexagonal close-packed high-entropy alloy: The effect of entropy. *Mater Des*. 2016;96:10–15.
- [14] Youssef KM, Zaddach AJ, Niu C, Irving DL, Koch CC. A novel low-density, high-hardness, high-entropy alloy with close-packed single-phase nanocrystalline structures. *Mater Res Lett*. 2015;3(2):95–99.
- [15] Feuerbacher M, Heidelmann M, Thomas C. Hexagonal high-entropy alloys. *Mater Res Lett*. 2015;3(1):1–6.
- [16] Gali A, George EP. Tensile properties of high- and medium-entropy alloys. *Intermetallics*. 2013;39:74–78.
- [17] Wang WR, Wang WL, Wang SC, Tsai YC, Lai CH, Yeh JW. Effects of Al addition on the microstructure and mechanical property of $\text{Al}_x\text{CoCrFeNi}$ high-entropy alloys. *Intermetallics*. 2012;26:44–51.
- [18] Tong CJ, Chen MR, Yeh JW, et al. Mechanical performance of the $\text{Al}_x\text{CoCrCuFeNi}$ high-entropy alloy system with multiprincipal elements. *Metall and Mat Trans A*. 2005;36(5):1263–1271.
- [19] Wang YP, Li BS, Ren MX, Yang C, Fu HZ. Microstructure and compressive properties of AlCrFeCoNi high entropy alloy. *Mater Sci Eng: A*. 2008;491(1–2):154–158.
- [20] Kumar N, Ying Q, Nie X, et al. High strain-rate compressive deformation behavior of the $\text{Al}_{0.1}\text{CrFeCoNi}$ high entropy alloy. *Mater Des*. 2015;86:598–602.
- [21] Komarasamy M, Kumar N, Tang Z, Mishra RS, Liaw PK. Effect of microstructure on the deformation mechanism of friction stir-processed $\text{Al}_{0.1}\text{CoCrFeNi}$ high entropy alloy. *Mater Res Lett*. 2015;3(1):30–34.
- [22] Zhu YT, Liao XZ, Wu XL. Deformation twinning in nanocrystalline materials. *Prog Mater Sci*. 2012;57(1):1–62.
- [23] Hemphill MA, Yuan T, Wang GY, et al. Fatigue behavior of $\text{Al}_{0.5}\text{CoCrCuFeNi}$ high entropy alloys. *Acta Mater*. 2012;60(16):5723–5734.
- [24] Zhang Y, Zuo T, Cheng Y, Liaw PK. High-entropy alloys with high saturation magnetization, electrical resistivity, and malleability. *Sci Rep*. 2013;3:1455–7.
- [25] Trexler MM, Thadhani NN. Mechanical properties of bulk metallic glasses. *Prog Mater Sci*. 2010;55(8):759–839.
- [26] T Mashimo RC. Transition to a Virtually Incompressible Oxide Phase at a Shock Pressure of 120 GPa (1.2Mbar): $\text{Gd}_3\text{Ga}_5\text{O}_{12}$. *Phys Rev Lett*. 2006;96(10):105504–4.
- [27] Turneaure SJ, Winey JM, Gupta YM. Compressive shock wave response of a Zr-based bulk amorphous alloy. *Appl Phys Lett*. 2004;84(10):1692–1694.
- [28] Togo H, Zhang Y, Kawamura Y, Mashimo T. Properties of Zr-based bulk metallic glass under shock compression. *Mater Sci Eng: A*. 2007;449–451:264–268.
- [29] Tian F, Delczeg L, Chen N, et al. Structural stability of NiCoFeCrAlx high-entropy alloy from ab initio theory. *Phys Rev B*. 2013;88(8):085128–5.
- [30] Tsai KY, Tsai MH, Yeh JW. Sluggish diffusion in Co–Cr–Fe–Mn–Ni high-entropy alloys. *Acta Mater*. 2013;61(13):4887–4897.
- [31] He JY, Liu WH, Wang H, et al. Effects of Al addition on structural evolution and tensile properties of the FeCoNiCrMn high-entropy alloy system. *Acta Mater*. 2014;62:105–113.
- [32] Zhuang S, Lu J, Ravichandran G. Shock wave response of a zirconium-based bulk metallic glass and its composite. *Appl Phys Lett*. 2002;80(24):4522–4524.
- [33] Martin M, Sekine T, Kobayashi T, Kecskes L, Thadhani NN. High-pressure equation of the state of a zirconium-based bulk metallic glass. *Metall Mat Trans A*. 2007;38(11):2689–2696.
- [34] Xi F, Yu Y, Dai C, et al. Shock compression response of a Zr-based bulk metallic glass up to 110 GPa. *J Appl Phys*. 2010;108(8):083537–5.
- [35] Marsh SP. LASL shock Hugoniot data: University of California Press, Berkeley, 1980.
- [36] Morris CE. Los Alamos shock wave profile data: University of California Press, Berkeley, 1982.
- [37] Strand OT, Goosman DR, Martinez C, et al. Compact system for high-speed velocimetry using heterodyne techniques. *Rev Sci Instrum*. 2006;77(8):083108–8.
- [38] Ahrens TJ, Gust WH, Royce EB. Material strength effect in the shock compression of alumina. *J Appl Phys*. 1968;39(10):4610–4616.
- [39] Dugdale JS, MacDonald DKC. The thermal expansion of solids. *Phys Rev*. 1953;89(4):832–834.
- [40] Meyers MA. Dynamic behavior of materials: John Wiley and Sons, New York, 1994.
- [41] Loree TR, Warnes RH, Zukas EG, Fowler CM. Polymorphism of shock loaded Fe-Mn and Fe-Ni alloys. *Science*. 1966;153(3741):1277–1278.
- [42] Yadav S, Chichili D, Ramesh K. The mechanical response of a 6061-T6 Al/Al₂O₃ metal matrix composite at high rates of deformation. *Acta Metall Mater*. 1995;43(12):4453–4464.
- [43] Murr LE. Metallurgical effects of shock and high-strain-rate loading, Elsevier, London, 1987.